Medical Image Analysis 13 (2009) 920–930

Contents lists available at ScienceDirect

Medical Image Analysis

journal homepage: www.elsevier.com/locate/media

Biomechanisms for modelling cerebral cortical folding

Guangqiang Geng [a,b,*], Leigh A. Johnston [a,c], Edwin Yan [d], Joanne M. Britto [a], David W. Smith [e], David W. Walker [f], Gary F. Egan [a,g]

[a] Howard Florey Institute, Florey Neuroscience Institutes, Level 2, Alan Gilbert Building, 161 Barry Street, Carlton South VIC 3053, Melbourne, Australia
[b] Graduate School of Biomedical Engineering, University of New South Wales, Sydney, NSW 2052, Australia
[c] Dept. of Electrical and Electronic Engineering, University of Melbourne and NICTA Victorian Research Laboratory, Parkville, VIC 3010, Australia
[d] National Trauma Research Institute, Alfred Hospital, PO Box 315, Prahran, VIC 3181, Australia
[e] Dept. of Civil and Environmental Engineering, University of Melbourne, Parkville, VIC 3010, Australia
[f] Dept. of Physiology, Monash University, Clayton, VIC 3800, Australia
[g] Centre for Neuroscience, University of Melbourne, Parkville, VIC 3010, Australia

ARTICLE INFO

Article history:
Received 1 April 2008
Received in revised form 30 November 2008
Accepted 5 December 2008
Available online 3 January 2009

Keywords:
Diffusion tensor imaging (DTI)
Cerebral cortical folding
Brain development
Biomechanical modelling

ABSTRACT

Understanding the biomechanical mechanisms by which the cerebral cortex folds is a fundamental problem in neuroscience. Current mathematical models of cortical folding do not include three dimensional geometry or measurement of cortical growth in developing brains extracted from experimental data. We present two biomechanical models of cortical folding which integrate 3D geometry and information taken from MRI scans of fetal sheep brains at a number of key developmental stages. The first model utilises diffusion tensor imaging (DTI) measurements of white matter fibre orientation in the fetal sheep brains as a cue to the tension forces that may regulate folding. In the second model, tangential cortical growth is modelled by osmotic expansion of the tissue and regulated by inhomogeneous white matter rigidity as a biomechanism of cortical folding. This is based on quantitative analysis of cortical growth and inhomogeneous white matter anisotropy measured from the MRI data. We demonstrate that structural and diffusion tensor MRI can be combined with finite element modelling and an explicit growth mechanism of the cortex to create biologically meaningful models of the cortical folding process common to higher order mammals.

1. Introduction

The cerebral cortex covers most of the superficial part of the mammalian brain. Folding of the cerebral cortex in human and higher mammals such as the baboon and macaque monkey is related to higher intelligence, such that the greater the degree of cortical folding, the more intelligent the species (Buettner-Janusch, 1963). Highly folded cortices are not restricted to primates, but are found also in other lineages such as the monotremes; the echidna cortex is gyrencephalic while the platypus is lissencephalic (Meyer, 2007). During the initial stages of brain development in the human embryo, a smooth cortex forms by cell migration from subcortical structures. At the fifth or sixth month of gestation, the cortex begins to fold, forming the gyri (outward folds) and sulci (inward folds) from this stage until after birth (Ottoson, 1983). The cortical folding increases the surface area of the cortex relative to the brain volume, and permits rapid increase of the cortical surface area during significant growth phases of the cortical volume (Richman et al., 1975).

The search for biomechanisms involved in cortical folding has been motivated by a desire to understand the folding pattern unique to each human brain, and by neurological disorders that result in abnormal cortical folding (Levine and Barnes, 1999), including Down's syndrome (Venita, 1996) and lissencephaly, in which the brain folds are less numerous and smaller than normal folds (Richman et al., 1975). Studies to-date have simulated cortical folding via mathematical formulation of mechanisms including elasticity and plasticity of the cortex (Raghavan et al., 1997; Toro and Burnod, 2005), differential growth of cortical layers (Richman et al., 1975), limitation of growth by the skull and white matter fibres (Raghavan et al., 1997), and modulation of tangential neuron migration by chemical activation and inhibition (Cartwright, 2002).

Current mathematical models do not incorporate experimental measurements of developing brains in terms of brain growth or the mechanical properties of brain tissue. Rather, these models formulate cortical growth either via a theoretical relationship that lacks physical meaning, or via an over-simplified model that is not able

* Corresponding author. Address: Howard Florey Institute, Florey Neuroscience Institutes, Level 2, Alan Gilbert Building, 161 Barry Street, Carlton South VIC 3053, Melbourne, Australia. Tel.: +61 3 8344 1883; fax: +61 3 9347 0446.
E-mail addresses: guangqiang.geng@florey.edu.au, geng45@pcomm.hfi.unimelb.edu.au (G. Geng).

1361-8415/$ - see front matter © 2008 Elsevier B.V. All rights reserved.
doi:10.1016/j.media.2008.12.005

to incorporate realistic biomechanical modelling or extend easily to 3D.

The hypothesis that cortico–cortico connections between highly interconnected cortical regions are regulatory factors in gyrus formation has not been tested (Van Essen, 1997), nor has anisotropy and heterogeneity in white matter tract formation been investigated as a mechanism of folding. Cortical growth has similarly not been thoroughly explored. It is generally accepted that the rapid increase in cortical surface area during development, exceeding the increase in available space beneath the cranium, causes folding of the cortical sheet. The 1000-fold increase in cortical surface area during mammalian evolution without a concomitant increase in cortical thickness has been hypothesised to have resulted from a change in proliferation kinetics that replicated cortical columnar units but did not alter the density of neurons within each column (Rakic, 1995). Interestingly, however, neuron migration and mitosis have largely finished by the gestational time at which the cortex begins to fold (Meyer, 2007), suggesting that the rapid tangential expansion is due to the genesis of glial cells, oligodendrocytes and astrocytes (Vaccarino et al., 2007), the innervation of axons and the formation of dense dendritic arbours.

In order to understand the regulation of cortical folding by biomechanical factors including the 3D developing cortical geometry, white matter fibre tension, anisotropic growth of the cortex and the inhomogeneous elasticity of the white matter, we propose 3D biomechanical finite element models that integrate geometry and measurements of developing brains from magnetic resonance imaging (MRI). Two biomechanisms of cortical folding are proposed. Firstly, tension forces applied by white matter fibres, as proposed by Van Essen (1997) as a regulation of cortical folding, are modelled based on observations from diffusion tensor imaging (DTI) (Basser et al., 1994). Specifically, fractional anisotropy (FA) and the direction of the principle eigenvector of diffusion (Pierpaoli and Basser, 1996) are used as a cues to white matter tension and direction. The magnitudes of the white matter fibre tension forces in developing brains are not currently known, and the cortex itself is extraordinarily elastic and substantially incompressible (Miller and Chinzei, 2002). In our second model, we propose cortical growth as a biomechanism of cortical folding. We have simulated cortical folding through a novel osmotic expansion model of the anisotropic growth of the cortex, regulated by inhomogeneous white matter rigidity. The growth parameters are based on measurements of developing brains from MRI data. Thermal expansion, equivalent to osmotic expansion, has been previously used to simulate the atrophy of human brain in dementia induced by Alzheimer's disease (Camara et al., 2006).

MRI measurements have been used in the study of human brain development, both in neonatal (Neil et al., 1998) and perinatal studies (Garel et al., 2001), and in a range of postmortem animal studies, from embryonic mouse (Zhang et al., 2003) to fetal baboon (Kroenke et al., 2007). We have chosen the fetal sheep brain as our experimental system, for its relatively simple gyrification pattern, size and availability.

The fetal sheep acquisition and subsequent measurements of cortical growth across a gestational period shown to encompass significant folding events are described in Section 2. In Section 3, the two mathematical models corresponding to two novel biomechanisms of cortical folding are described that incorporate the cues from the experimental data. In Section 3.2, the deformation of a smooth 70 day cortical geometry, extracted from the MRI data, is computed via a dynamic solid stress–strain model with loading of white matter tension force. The cortical growth, simulated as an anisotropic osmotic expansion, is integrated with the stress–strain model in Section 3.3. The inhomogeneous elasticity of white matter, indicated by inhomogeneous fractional anisotropy in the experimental sheep brain data, regulates the cortical folding in this model. In Section 4, results of simulations of the white matter tension model and the cortical growth model are presented, followed by the discussion and conclusion, in Section 5 and 6, respectively.

2. Experimental data

2.1. Preparation of fetal sheep brains

Fetal sheep brains were extracted at the relevant gestational time points. Each fetus was perfused transcardially with 500–1000 ml of heparinized saline according to the size of the fetus, followed by the same volume of 4% Paraformaldehyde (PFA). The brain was subsequently removed from the fetus, and was placed in 4% PFA at least 48 h before the MRI scan.

2.2. Acquisition of MRI data

A set of fetal sheep brains at 70, 80, 90, 110 and 130 days of gestation (Fig. 1) were scanned at high resolution on a Brüker Biospec 4.7T MRI scanner. T2-weighted and diffusion weighted imaging (DWI) data were acquired for each of the brains via a multislice multiecho sequence and a standard DTI sequence. Coronal slices of 1 mm thickness with in-plane resolution of 0.258×0.258 mm^2 were acquired perpendicular to the anterior–posterior commissure line. For the 70 and 80 day brains, the imaging matrix was $128 \times 128 \times 30$ (Fig. 1a and b), while the imaging matrix was $256 \times 256 \times 45$ (Fig. 1c, d and e) for the 90, 110 and 130 day brains due to the increased brain size. (TE = 50 ms for all brains, TR = 4 s for the 70 and 80 day brains; TR = 10 s for the 90, 110 and 130 day brains). Twelve-direction DWI data were acquired following the T2-weighted scan with the same matrix size, spatial resolution, TE and TR, with a b-value of 1000 s/mm^2.

2.3. Measurement of cortical growth

In order to understand the cortical growth characteristics in the fetal sheep brain, cortical surface area, mean cortical thickness and number of sulci were measured from the acquired MR data. Though measurement of the same brain at different developmental stages would be ideal, in utero MRI acquisition is extremely difficult. Given the simple folding pattern of sheep cortex, we made the assumption that the primary sulci and gyri are stable across individual sheep brains.

Cortical surfaces were reconstructed from MR data using Freesurfer (Dale et al., 1999; Fischl et al., 1999) with the reconstruction parameters adapted for processing fetal sheep rather than human brain data. Each brain was manually segmented from the 2D MR slices, and the edges of segmented brain boundary voxels were taken as edges of an initially reconstructed 3D brain surface mesh. The initial mesh was smoothed to remove boundary artifacts between 2D slices.

The mean cortical thickness was measured in the middle slice of the volume. Left and right segments with the optimal contrast between the cerebral cortex and white matter in each brain were chosen between the longitudinal cerebral fissure, which separates the left and right hemispheres, and the left and right Sylvian sulci.

Fig. 2 displays the increase in cortical surface area and mean cortical thickness across time. The cortical surface area increased 7.6 times from the smooth 70 day brain (Fig. 1a) to the 130 day brain (Fig. 1e), while the cortical thickness increased only 1.6 times during the same period. The significantly greater increase of corti-

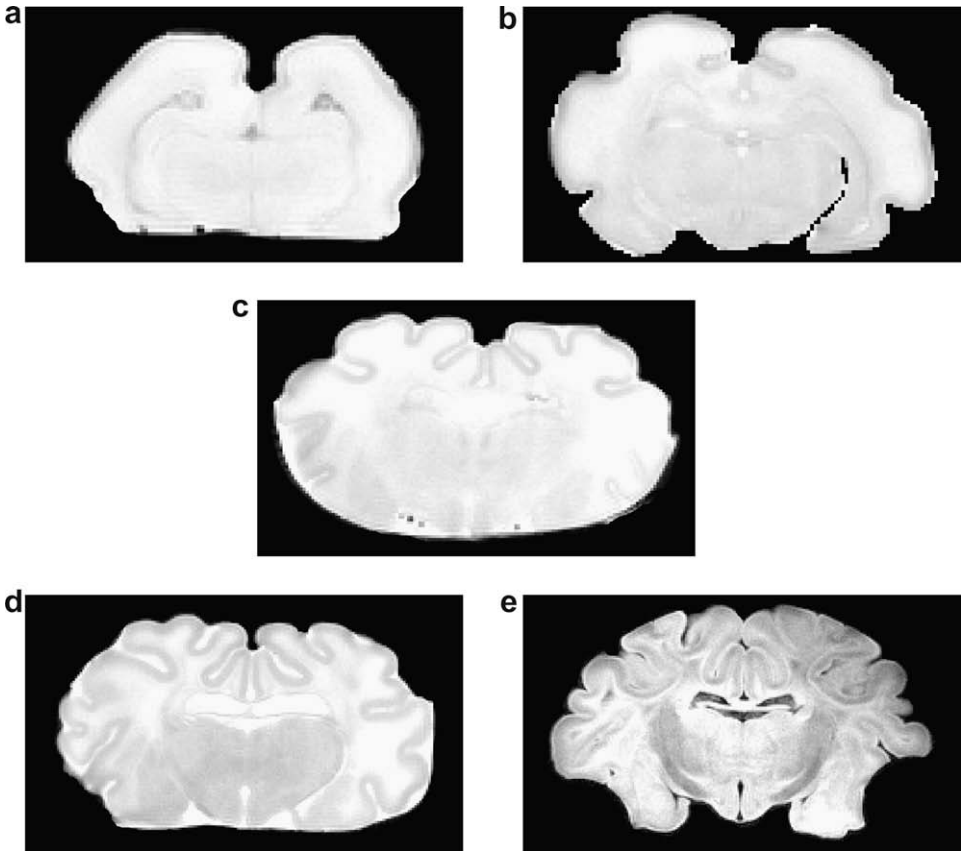

Fig. 1. Slices of T2-weighted MRI of fetal sheep brain at (a) 70, (b) 80, (c) 90, (d) 110 and (e) 130 days gestation.

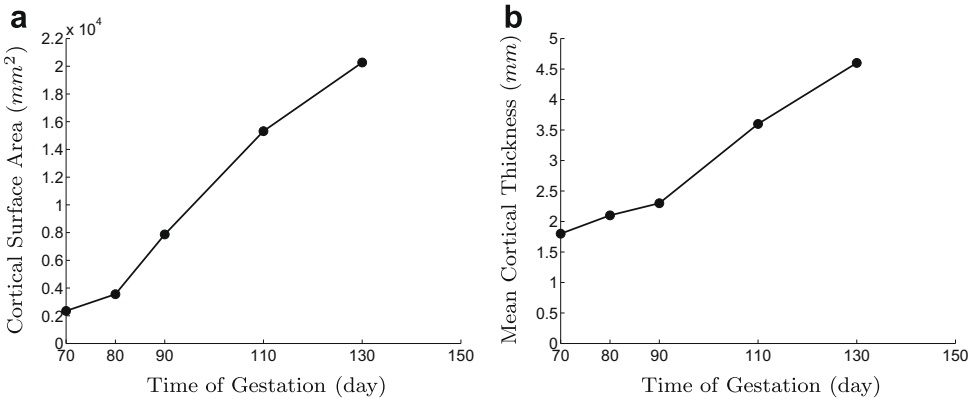

Fig. 2. Increase of (a) cortical surface area and (b) mean cortical thickness measured from MRI data.

cal surface area compared to mean cortical thickness indicates that the expansion of the cortical volume tangential to the cortical surface is significantly greater than the radial expansion. This anisotropic cortical growth is taken into account in our second biomechanical model of cortical folding in Section 3.3.

The surface of the 70 day brain was smooth with only a few shallow dimples, while by 130 days, the cortical surface had undergone significant gyrification. Fig. 3 plots the number of sulci over time. The greatest increase in the number of sulci occurred between 70 and 90 days gestation, with significant folding initiating between 70 and 80 days (Fig. 1a and b). For this reason, we focussed on modelling the geometric deformations that occur between 70 and 90 days (Section 3.2).

2.4. Measurement of diffusion fractional anisotropy

The fractional anisotropy (FA) was measured from the DTI data (Pierpaoli and Basser, 1996), as a measure of variability of white matter diffusivity. Fractional anisotropy is a metric of water molecule diffusion anisotropy, which is induced by restriction of diffusion perpendicular to the white matter fibres. Higher FA generally corresponds to greater fibre myelination which increases during brain development (Neil et al., 1998), and surrogate makes greater rigidity of white matter along fibre directions in myelinated white matter regions.

The mean diffusion FA within a three voxel radius neighbourhood was measured for each voxel in the white matter extending

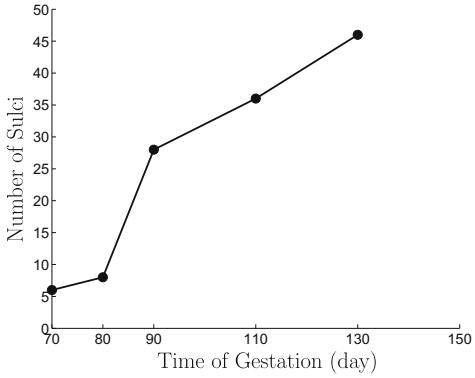

Fig. 3. Number of sulci in the fetal sheep brain as a function of gestational age.

from the cingulate sulcus to the Sylvian sulcus of each hemisphere, and parallel to the boundary between the cortex and the white matter, as depicted by the yellow skeleton curves in Fig. 4a. As is shown in this figure, the cortical region between the cingulate sulcus and the Sylvian sulcus was smooth in the 70 day brain, in contrast to the appearance of the middle sulcus at the same region in the 80 day brain (Fig. 4b).

Fig. 5 shows the mean FA of the white matter along the left and right skeleton curves in the 70 day brain, respectively. The mean FA is markedly lower at the points where the middle sulci appear in the 80 day brain (Fig. 4b). Similarly, the mean FA displays local minima at points in the white matter beneath the cingulate and Sylvian sulci, which are shallow dimples at 70 days and have folded deeper at 80 days.

3. Finite element models of cortical folding

To investigate potential biomechanisms of cortical folding, simulations of two biomechanical models were conducted. In the first model of cortical folding (Section 3.2), simulated white matter fibre tension forces were applied via a dynamic stress–strain model under large deformation. The second model (Section 3.3) formulates cortical growth as a osmotic expansion in an analogous way to modelling thermal expansion, in addition to the deformation stress–strain model. Based on our measurements of cortical growth and the diffusion FA in white matter from the MR data, together with published values of brain tissue rigidity, we simulated anisotropic cortical growth and inhomogeneous white matter rigidity as mechanisms of cortical folding.

3.1. Finite element model formalism

Due to the dynamic and significant deformation involved in cortical folding, both models are formulated as time-dependent large deformations. The second Piola Kirchhoff stress, **S**, and Green–Lagrangian strain tensor, ϵ, are used as measurement of the stress and strain internal to the cortex (Fung, 1993). The second Piola Kirchhoff stress is

$$\mathbf{S} = J\mathbf{F}^{-1} \cdot \boldsymbol{\sigma} \cdot (\mathbf{F}^{-1})^{\mathrm{T}} \tag{1}$$

where **F** is deformation gradient tensor, J is the Jacobian of **F**, and $\boldsymbol{\sigma}$ is Cauchy stress defined as the force per unit area in the deformed geometry. The (i,j) element of Green–Lagrangian strain tensor is

$$\epsilon_{ij} = \frac{1}{2}\left(\sum_{k=1}^{3} \frac{\partial x_k}{\partial a_i}\frac{\partial x_k}{\partial a_j} - \delta_{ij}\right). \tag{2}$$

Here $\mathbf{a} = [a_1, a_2, a_3]$ and $\mathbf{x} = [x_1, x_2, x_3]$ are coordinates of the original and deformed positions, respectively, and $\delta_{ij} = 1$ iff $i = j$.

The principle of virtual work evolves the geometry (Boresi and Chong, 1987), and is expressed as

$$\int_{\mathscr{S}} S_{ni}\delta u_i dS + \int_{\mathscr{V}} B_i \delta u_i dV - \int_{\mathscr{V}} \rho \ddot{u}_i \delta u_i dV = \int_{\mathscr{V}} S_{ji}\delta\epsilon_{ij} dV \tag{3}$$

where the four terms in (3) are the virtual work done by the surface stress force, the external body force, the inertial force and the internal force, respectively. S_{ni} and B_i are the stress force normal to the surface and the external body force respectively, ρ is mass density, $u_i = x_i - a_i$ is the displacement, δu_i is the virtual displacement, and $\ddot{u}_i$ is acceleration.

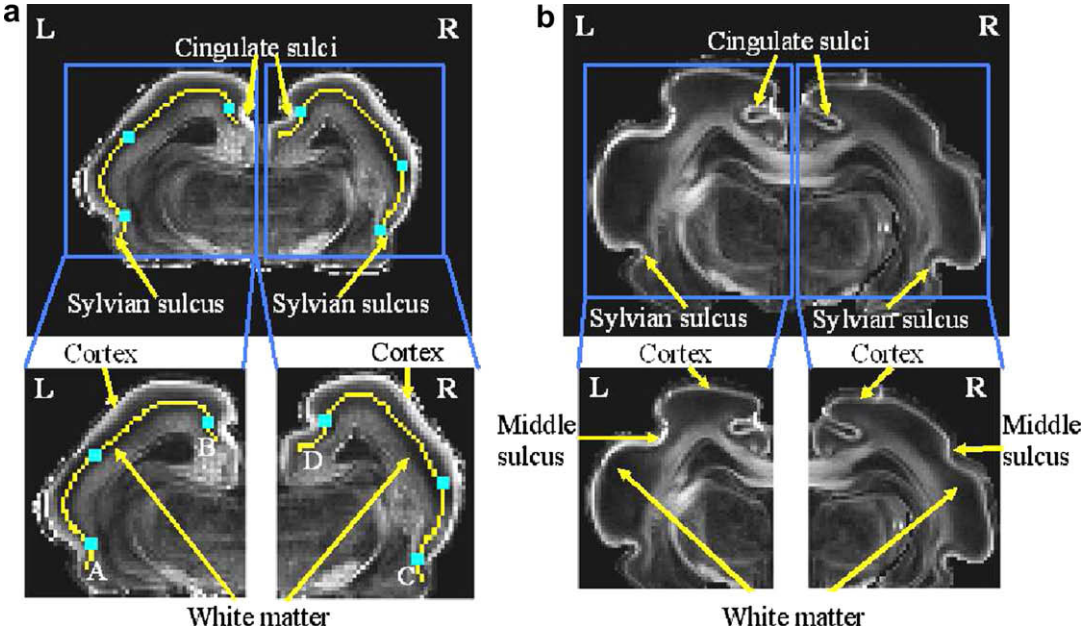

Fig. 4. Slices of (a) 70 day and (b) 80 day brain FA images for mean FA measurement. Left and right insets show selected regions. Cyan squares in (a) show positions of FA local minima. A, B, C and D are the voxels indexing beginning and end of skeleton curves (yellow) in left and right hemispheres, respectively. (For interpretation of the references to color in this figure legend, the reader is referred to the web version of this article).

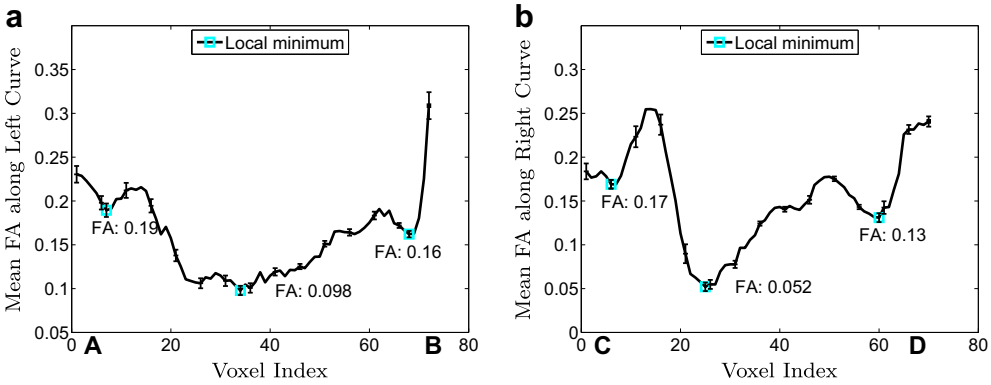

Fig. 5. Mean FA along (a) left and (b) right hemisphere skeleton curves in white matter at 70 days. Standard errors displayed every five voxels. Cyan squares show local minima in FA. (For interpretation of the references to color in this figure legend, the reader is referred to the web version of this article.)

As an extension to the previously proposed non-growth model (Geng et al., 2007), cortical growth is formulated as an osmotic expansion in an analogous way that a thermal expansion is modelled in a heated plate, which has been previously used to simulate the atrophy of human brain in dementia induced by Alzheimer's disease (Camara et al., 2006). In a heated plate, the increased thermal agitation of the molecules leads to an increase in volume of the material, which may lead to buckling of the plate. In the same way, an increase in the osmotically actively particles per unit volume of the cortex (induced by an increase in the number and size of cells, support structures and dendritic trees during cortical growth), leads to an expansive osmotic pressure within the cortex. We postulate that this osmotic expansion contributes to cortical folding such that the same mathematical formalism may be employed to model both thermal expansion and osmotic expansion.

$$\frac{\partial O}{\partial t} = Q \tag{4}$$

where O is osmotic particle density, that is the number of osmotically active particles per unit volume, and Q is the production rate of osmotically active particles per unit volume.

The change in osmotic particle density, ΔO, induces osmotic expansion, which is coupled with the mechanical deformation in (3) through addition of osmotic expansion strain into the constitutive equation, as follows:

$$\mathbf{S}_{\text{vec}} = \mathbf{D}(\boldsymbol{\epsilon}_{\text{vec}} - \boldsymbol{\epsilon}^{O}_{\text{vec}}) \tag{5}$$

where $\mathbf{S}_{\text{vec}}$ and $\boldsymbol{\epsilon}_{\text{vec}}$ are vector forms of stress and strain tensors, respectively. $\mathbf{D}$ is the stiffness matrix, formed from the biomechanical properties of gray and white matter. $\boldsymbol{\epsilon}^{O}_{\text{vec}}$ is osmotic expansion strain vector,

$$\boldsymbol{\epsilon}^{O}_{\text{vec}} = \boldsymbol{\alpha}_{\text{vec}} \Delta O \tag{6}$$

where $\boldsymbol{\alpha}_{\text{vec}} = [\alpha_x, \alpha_y, \alpha_z, 0, 0, 0]$ is the vector of osmotic expansion ratios for the orthogonal material property assumed in this study (Fung and Tong, 2001, Chapter 12).

The cortical tissue constitutive relationship (5) is assumed to be linear to simplify the problem, following the linear formulation of elastic material properties applied in neurosurgical simulation of human brain deformation (Warfield et al., 2000).

3.2. White matter tension model

3.2.1. Cortical mesh construction

Due to the inherent computational complexity of simulating the full cortex, we have confined the model to 3D cortical ribbons extracted from individual sections from the MRI data volume. To extract each 3D cortical ribbon from each image volume, a dorsal segment of the brain, between the longitudinal cerebral fissure which separates the left and right hemispheres and the Sylvian sulcus of the left hemisphere, was selected, as shown in Fig. 6. The cortical ribbon was manually delineated across slices within each brain segment and saved as a binary image mask. The 2D cortical contour was extracted from each slice of the volume, and using COMSOL Multiphysics,[1] a 3D volumetric geometry was produced through filling and lofting together the 2D geometries. The COMSOL meshing feature was used to generate meshes for the cortical geometries with Lagrange–Quadratic tetrahedral elements.

3.2.2. Biomechanical properties

Experimental measurements of the elastic properties of fetal sheep brain are not available. A Young's modulus value of 2.1×10^5 N/m^2 was used together with a Poisson's ratio of 0.45 (Gao et al., 2006) in order to formulate an initial and qualitative simulation. These parameter choices were necessary to obtain simulated folding, possibly due to incomplete modelling of forces, particularly the tangential forces simulating growth.

3.2.3. Loading and constraints

The cortical surfaces were categorized into three surfaces, with different loadings and constraints for displacement: the exterior surface, the interior surface, and the anterior and posterior surfaces. The exterior surface is the boundary between the cortex and cerebral-spinal fluid (CSF), onto which an inward pressure force was applied by the CSF with a spatially homogeneous distribution (Fig. 7c). The CSF pressure was set according to experimental measurement (Neville and Egan, 2005) to be 2000 N/m^2 normal to the surface (Table 1).

The interior surface is the boundary between the cortex and white matter fibres, with the latter postulated to apply tension forces to the cortex (Van Essen, 1997). The interior surface is divided into the central (yellow in Fig. 7a) and lateral (green in Fig. 7a) surfaces. Based on the observation that the principle eigenvector of the diffusion tensor reconstructed from the DWI data for the 70 day brain lies perpendicular to the gray/white interface, as shown in Fig. 8, the direction of the force applied from white matter fibres onto the interior surface of the cortex was set to be normal to the local surface, in agreement with Hilgetag and Barbas's observation in the rhesus brain (Hilgetag and Barbas, 2005).

We specified two loading conditions for the interior surface (Fig. 7). The loadings and constraints for these two scenarios are shown in Table 1. Firstly, the magnitude of pressure on the interior surface was set to be 4000 N/m^2 (Table 1, Scenario 1), doubles the

[1] http://www.comsol.com/.

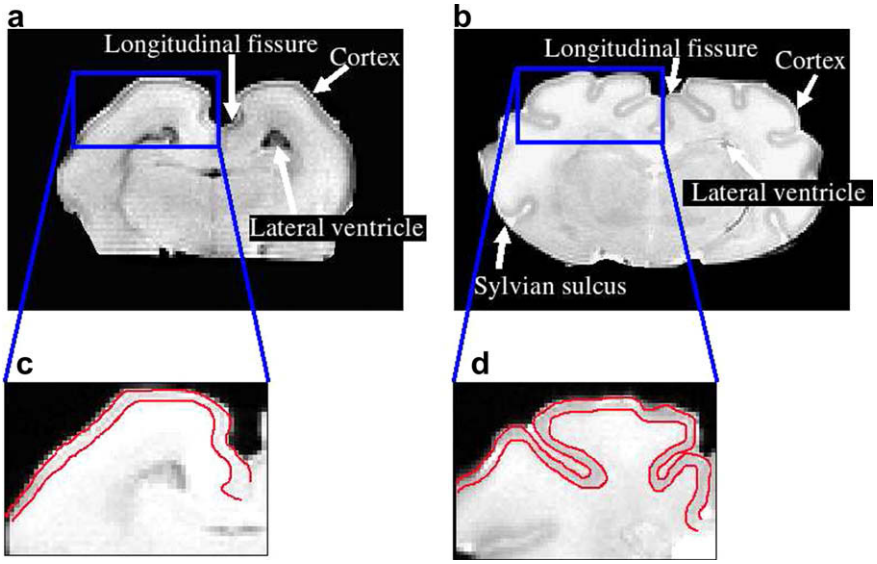

Fig. 6. Coronal slices of (a) 70 day and (b) 90 day brain; T2-weighted MRI. Manually delineated boundaries of cortical ribbons for (c) 70 and (d) 90 day brain.

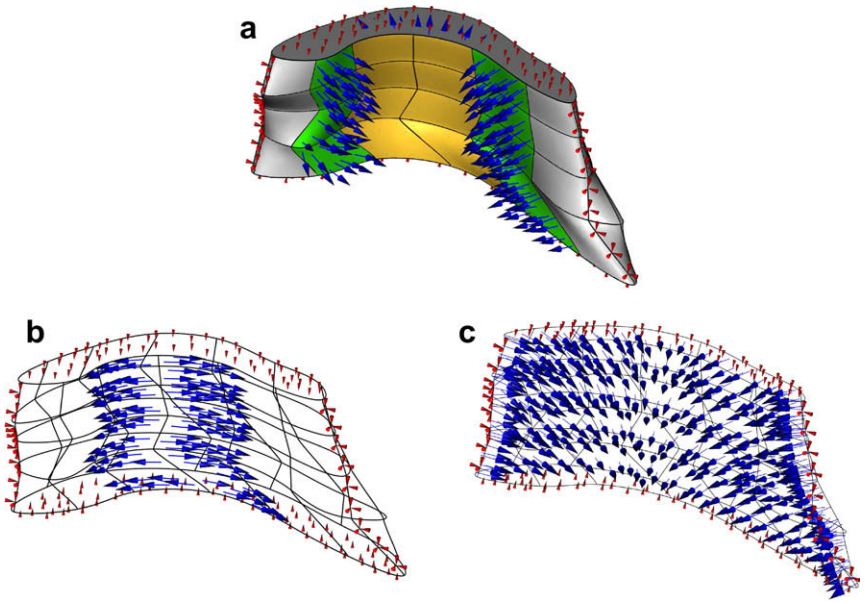

Fig. 7. Loadings and constraints. Blue arrows: loadings. Red arrows: constraints. (a) Loading of white matter tension force. (b) Loading of tangential force. (c) Loading of CSF pressure. (For interpretation of the references to color in this figure legend, the reader is referred to the web version of this article.)

Table 1
Loadings and constraints. Anterior and posterior surfaces were fixed.

Scenario number	Force direction	Interior surface force (N/m^2)		Exterior surface force (N/m^2)
		Central	Lateral	
1	Radial	4000 (outward)	4000 (inward)	2000 (inward)
	Tangential	0	0	0
2	Radial	3000 (outward)	4000 (inward)	2000 (inward)
	Tangential	1000	0	0

magnitude of the CSF pressure. This magnitude was chosen to be of the same order as the CSF pressure as no values for the magnitude of the white matter fibre tension in developing brains are available. Inward folding at the lateral interior surfaces was simulated with an inward white matter fibre tension force, consistent with Van Essen's white matter tension-based hypothesis (Van Essen, 1997). To simulate this, the force was formulated to be inward at the lateral interior surfaces (green in Fig. 7a) in the model. The outward

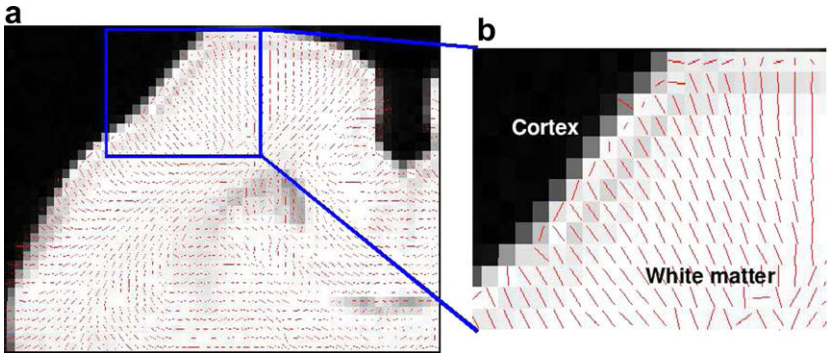

Fig. 8. (a) Principle diffusion tensor eigenvectors (red) overlaid on T2-weighted image. (b) Zoomed section displaying homogeneous distribution of principle eigenvectors perpendicular to the boundary between cortex and white matter. (For interpretation of the references to color in this figure legend, the reader is referred to the web version of this article.)

movement of the central interior surface was simulated by a net outward force, that was assumed to result from the outward force simulating growth being greater than the comparably lower inward force simulating the white matter fibre tension. In consequence, the net force was simulated as an outward force normal to the central interior surface (yellow in Fig. 7a).

In the second scenario (Table 1, Scenario 2), a force with a pressure magnitude of 1000 N/m^2 was applied tangential to the central interior surface (Fig. 7b), and the normal pressure was reduced to 3000 N/m^2 in order to prevent over-compression of the cortex. This was to simulate the effects of tangential growth of the cortex via a tangentially applied force on the interior surface of the cortex. The tangential force is an indirect way of simulating the tangential growth of the cortex.

The anterior and posterior surfaces of the cortical region are the boundaries between different parts of the cortex. To limit the spatial domain of the problem within the cortical region extracted, no loading was applied to these two surfaces, and displacement normal to these two surfaces was inhibited. For the same reason, the ends of the cortical region were fixed to prevent displacement. A Rayleigh damping force was applied with a mass damping of 1 s^{-1}, and a stiffness damping of 0.001 s.

3.2.4. Solution of equations

The iterative generalized minimal residual (GMRES) solver with incomplete lower-upper (LU) factorization preconditioner for non-symmetric matrix problems was selected from the COMSOL Multiphysics modules to solve for the deformation of the geometry of the 70 day cortical region. The simulations were stopped explicitly to compare to the 90 day cortical region. The simulations were conducted on a 2.4 GHz PC with 2.5 GB memory. The computation of the deformation of the 70 day cortical region took 5–6 h. Although simulation on the actual time scale of a gestational period is planned, further investigations are required to determine correspondingly reduced magnitudes of loading pressures.

3.3. Cortical growth model

We now describe our formulation of the cortical growth model.

3.3.1. Formulation of cortical geometry

3D plates were used to represent the cerebral cortex and the white matter as an initial geometry for simulating the deformation during brain development (Fig. 10). The requirement for extra computational power used to couple osmotic expansion with the principle of virtual work did not allow us to simulate a more complicated geometry extracted from the MRI data. To make the size of the simulated geometry comparable to the real geometry, the size of the cortical region and the thickness of the underneath white matter were measured from the 70 day brain data (Fig. 9). The minimum white matter thickness, measured as the distance between the cortical region and the lateral ventricle (black arrow in Fig. 9), was shown to be more than double the cortical thickness.

In Fig. 10, the *xy* plane corresponds to the tangential directions, and the *z*-axis the radial direction, within the cortex. The top layer (gray) is the cortex with thickness 0.8 mm, while the bottom layer (Fig. 10, blue and green regions) is the white matter (1.6 mm), formulated following measurement of the actual brain geometry in the 70 day brain. Each layer consists of three horizontally square blocks. The length and width of each block were both 2 mm, resulting in a total $6 \times 2\ mm^2$ surface geometry. The geometry was meshed to 6884 tetrahedral elements. The number of elements

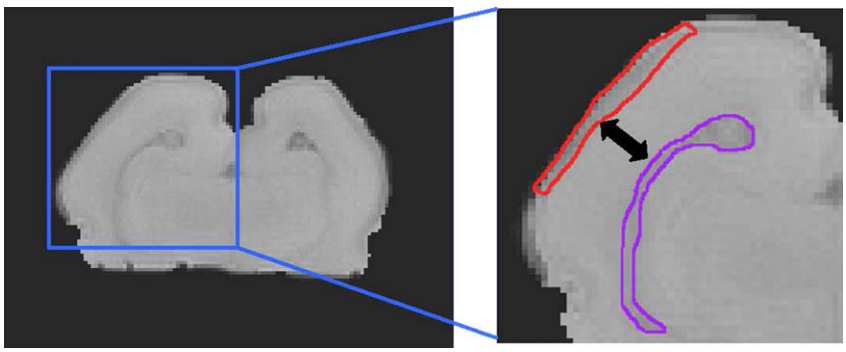

Fig. 9. Size of simulated 70 day brain segment. Arrow shows distance between boundaries of cortex (red) and lateral ventricle (purple) as white matter thickness. (For interpretation of the references to color in this figure legend, the reader is referred to the web version of this article.)

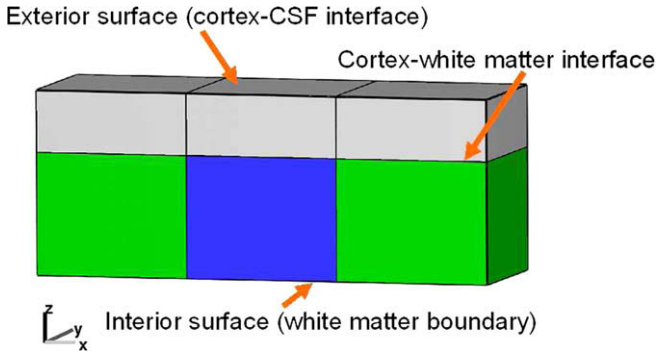

Fig. 10. Simulated geometry of the cortical growth model showing the cortex (gray), the central/sub-sulcal region of the white matter (blue), and the lateral/sub-gyral regions of white matter (green). (For interpretation of the references to color in this figure legend, the reader is referred to the web version of this article.)

Table 2
The material properties of the cortex and white matter used in the cortical growth model (Taylor and Miller, 2004).

Mechanical Properties		Cortex	White matter (sub-sulcal)	White matter (sub-gyral)
Young's modulus (N/m^2)		584.4	194.9	584.4
Shear modulus (N/m^2)		194.9	65.0	194.9
Osmotic expansion ratio α_{vec} (m^2/mol)	x	7.0×10^{-4}	0	0
	y	7.0×10^{-4}		
	z	0		
Poisson's ratio		0.499	0.499	0.499
Mass density (kg/m^3)		1.0×10^3	1.0×10^3	1.0×10^3

in the mesh of the cortical growth model was less than the white matter tension model, due to the simpler geometry of the second model, and the extra computational resources required for coupling osmotic expansion with the principle of virtual work.

3.3.2. Biomechanical properties

To simulate anisotropic cortical growth, we specified anisotropic osmotic expansion and biomechanical parameters as listed in Table 2. We used the relevant values for human brain properties, with a Young's modulus of 584.4 N/m^2, and a Poisson ratio of 0.499 (Taylor and Miller, 2004). These properties have been used in the simulation of hydrocephalus in human brain (Taylor and Miller, 2004), which is a slow brain deformation process within a time scale similar to cortical folding process during development. The rigidity of white matter was heterogeneous to simulate inhomogeneous myelination of neural fibres in sub-gyral and sub-sulcal regions of white matter, as evidenced in the experimental results of lower FA in sub-sulcal regions (Section 2.4). In the sub-sulcal white matter (green in Fig. 10), the Young's modulus was chosen to be 194.9 N/m^2, less than the Young's modulus in the sub-gyral white matter (584.4 N/m^2). This is based on our FA measurement results, in which the average FA in the sub-sulcal white matter was reduced approximately 60% compared to the FA in the sub-gyral white matter (Fig. 5). The shear modulus was computed from the relationship linking Young's modulus and Poisson's ratio, $G = E/2(1+\nu)$ (Altenbach et al., 2004).

Based on comparison of cortical growth in tangential and radial directions measured from the experimental data (Fig. 2), the tangential growth is significantly greater than the radial growth. To simulate this, the osmotic expansion of cortex is limited to be within the xy plane, while the osmotic expansion ratio along the z-axis is set to zero as a simplified simulation of less significant increase of cortical thickness compared to cortical growth tangential to its surface. The osmotic expansion ratio is lower than that is used by Camara et al. (2006) in simulating the atrophy of human brain in dementia induced by Alzheimer's disease, which ensures the numerical stability for our simulations.

3.3.3. Loading and constraints

The geometry's surface is categorized into three surfaces, the exterior surface, the interior surface and the surrounding surfaces including anterior, posterior, left and right faces of the geometry (Fig. 10). The exterior surface is the boundary between the cortex and CSF, while the interior surface is the boundary between different regions of the white matter.

3.3.4. Solution of equations

The iterative GMRES solver with incomplete lower-upper (LU) factorization preconditioner for non-symmetric matrix problems is again selected from the COMSOL Multiphysics modules to solve for the deformation. The computation lasted 1–2 h on a 2.4 GHz PC. Although simulation on the actual time scale of a gestational period is planned, further investigations are required to determine correspondingly reduced magnitudes of the heating expansion ratio.

4. Results

4.1. Simulation of white matter tension model

The 3D geometries of the 70 (Fig. 7) and 90 (Fig. 11c) day cortical regions were extracted from T2-weighted MRI data. The 70 day mesh, initially consisting of 2902 elements, was refined to 11,199 tetrahedral elements.

As described in Section 3.2, we formulated two scenarios without and with tangential force, respectively. The resultant geometries of the folded cortical region are shown in Fig. 11, with the actual measured 90 day brain region in Fig. 11c. The cortical thickness was different in the sulci and gyri, as summarised in Table 3. There was an increase in cortical thickness at the two lateral inward folds compared to a homogeneous cortical thickness of

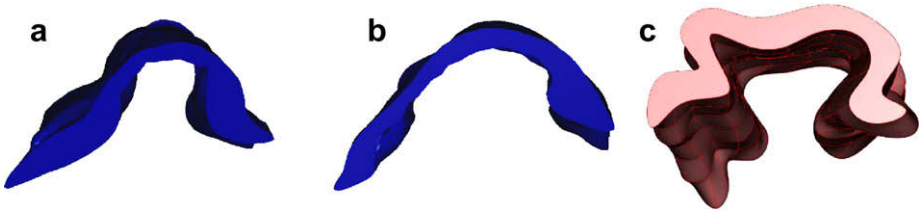

Fig. 11. Results of the white matter tension model showing (a) the simulated cortical folding without the inclusion of tangential force, and (b) the simulated cortical folding with the addition of tangential force. (c) The cortical ribbon extracted from the T2-weighted MRI data of the 90 day fetal sheep brain.

Table 3
Cortical thickness in gyri and sulci for simulated and experimental geometry.

	Gyri (mm)	Sulci (mm)			Ratio (gyri/sulci)
		Left	Right	Mean	
No tangential force	1.01	1.29	1.63	1.46	0.69
With tangential force	1.00	1.15	1.63	1.39	0.72
90 Day geometry	1.07	1.81	1.90	1.86	0.58

1.09 mm within the 70 day cortical region. This is due to the compression of the central part of the cortex by the CSF pressure from the exterior surface and the normal outward force from the central interior surface. At the two lateral inward folds, the normal force pulled inwards the lateral interior surfaces of the cortex away from its exterior surface.

The application of a tangential force on the central interior surface resulted in more realistic geometry (Fig. 11b) with a broader gyral section as in the real 90 day cortical region. There was a larger change in cortical thickness for the simulation with tangential force compared to the result without tangential force (Table 3) both in gyri and sulci. The change in cortical thickness resulting in both scenarios was less than that of the 90 day cortical geometry in both gyri and sulci. This is due to the limitation of the model in that cortical growth was not explicitly simulated.

4.2. Simulation of cortical growth model

Cortical growth was analogously formulated as an osmotic expansion, with a $2.50 \times 10^{-3} m^{-3} s^{-1}$ rate of change in the osmotically active particle density. Tangential expansion of the cortex resulted from setting the osmotic expansion ratio along the radial direction to zero. No CSF pressure or other loading was applied. As is shown in Fig. 12, the downward deformation along the z-axis (to a maximum deformation of 0.3 mm), possibly corresponding to an inward cortical fold, was greater at the central region compared to lateral regions of the geometry. The boundary (Fig. 12, coloured yellow) between the cortex and the white matter, with an initial z coordinate of 1.6 mm, was lower at the central region compared to the lateral regions of the geometry. The top boundary (Fig. 12, coloured red), which simulated the cortex-CSF interface, was markedly lower in the central region compared to the lateral regions of the geometry (to a maximum difference of 0.6 mm). This resulted from the relatively reduced rigidity along z direction in the central region compared to the lateral regions (Table 2).

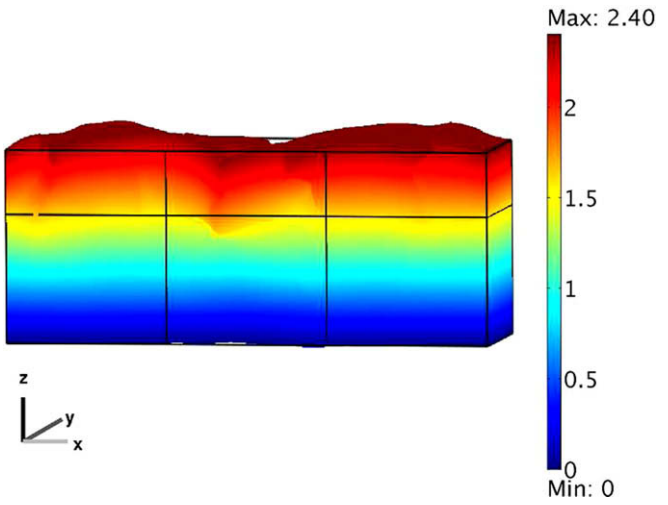

Fig. 12. Simulated geometry of model with cortical growth via osmotic expansion and non-homogeneous white matter rigidity. The colour encodes z coordinate at the beginning of the simulation.

5. Discussion

In order to simulate the biomechanisms of cortical folding, we have presented two finite element models, the white matter tension model and the cortical growth model. These two models employ the principle of virtual work that has been previously used in simulations of human brain deformation (Wittek et al., 2007). In the white matter tension model, the folding of each 3D cortical ribbon extracted from the MRI data was simulated by two strongly interconnected regions being pulled towards each other under the tension of the white matter fibres, as suggested by Van Essen's tension-based hypothesis (Van Essen, 1997). In contrast to the white matter tension model, the cortical growth model combines the principle of virtual work with explicitly modelled growth via osmotic expansion, as in the simulations of dementia induced atrophy in Camara et al. (2006).

The simulations of the white matter tension model demonstrate a 3D geometry resultant from the computation of cortical deformation that is qualitatively similar to the geometry directly extracted from MR volumetric data of a folded cortical region in a 90 day fetal sheep brain. The simulated change in cortical thickness between the gyral and sulcal regions is consistent with the experimental measurements from the 90 day cortical region. In this model, the principle eigenvector direction of the diffusion tensor qualitatively indicates the orientation of the simulated white matter fibre tension force. A quantitative formulation is still to be fully determined. Future studies using high angular resolution diffusion imaging (HARDI) data will enable better determination of the orientation of the diffusivity eigenvector directions. Application of tangential tension at the interior surface of the cortical region resulted in broader outward folding as well as a further decrease in cortical thickness, which resulted in the simulated geometry being more similar to the experimental cortical region than in the case without tangential tension. Hilgetag and Barbas (2005) have suggested this deformation to be a result of the normal compression onto the deep layers of the cortex induced by the tangential tension applied on the superficial layer of the cortex. It is not possible, however, to quantify the magnitude of the white matter fibre tension from DTI data. We used a value of Young's modulus larger than might be expected for actual fetal sheep brain tissue properties, which is a limitation of our simulation results for the white matter tension model. Brain structures such as the pia matter and factors such as the relative growth of the skull versus the cortex were not included in the white matter tension model, which could potentially affect the simulation results of cortical folding. Using a reduced Young's modulus of the order of values used in Taylor and Miller (2004) did not result in appreciable simulated folding, possibly due to incomplete simulation of the forces, in particular tangential forces in the cortex that may be critical to simulating cortical growth. A complete simulation of the magnitude and distribution of the white matter tension model forces was not possible as we did not perform direct measurement of the forces, and no other experimental results are available for developing brains.

This need for explicit cortical growth led to the development of the cortical growth model, specifying anisotropic cortical growth and heterogeneous anisotropy of the white matter, as observed in MRI data of the fetal sheep brain at 70 days prior to the formation of the middle sulcus. The Young's modulus and Poisson's ratio were chosen with reference to simulations of hydrocephaly in the human brain, which is a slow process similar to brain development (Taylor and Miller, 2004). The size and thickness of the cortical geometry were chosen based on measurements from the experi-

mental MRI data of the 70 day cortex. We demonstrated a correspondence between the appearance of the middle sulcus in the 80 day brain as well as the in-depth folding of the cingulate and Sylvian sulci, and the existence of local minima in the white matter FA in the 70 day brain. This suggests that heterogeneous unmyelinated white matter, as measured by diffusion FA (Neil et al., 1998), may provide a mechanism of inward cortical folding during growth due to relatively less rigidity in sub-sulcal regions. That is, white matter inhomogeneous anisotropy in the developing brain may produce variable damping effects upon which cortical growth occurs, leading to the formation of sulci. This reasoning is attractive, as it implicitly describes folding via formation of the sulci, rather than sulci developing as a by-product of gyrus formation, as the tension-based hypothesis of Van Essen (1997) would imply. Sulcal roots have been proposed as primary invariant features of folding patterns (Cachia et al., 2003; Mangin et al., 2004).

In simulating cortical growth, we modelled the increase of the tangential size of the cortex as an osmotic expansion under constant production rate of osmotically active particles. This formulation of cortical growth obviates the need for application of external forces. In particular, despite the tension-based hypothesis of Van Essen (1997), it is not known whether unmyelinated white matter places tension forces on the cortex, or whether the developing white matter tracts are more flexible. Growth, on the other hand, is generally accepted to be the primary cause of cortical folding (Todd, 1982). There have been a number of in situ and in vitro studies which compare brain tissue rigidity between adult and infant animal models such as porcine and rat (Thibault and Margulies, 1998; Prange and Margulies, 2002; Gefen et al., 2006). Significant differences in brain tissue rigidity have been shown in infants compared to adult brains under small strain. Currently available measurements of the mechanical properties of brain tissues have been acquired perinatally rather than during the gestational period that has been investigated in this study. In current work we are building more comprehensive empirical models of the cortical growth, which also capture the growth of the white matter. Future simulations with improved computational capability will enable the application of the cortical growth model to a more realistic and expansive cortical sheet geometry.

We have used the linear constitutive properties of brain tissues to undertake a qualitative simulation of brain deformation during cortical folding. Linear constitutive properties of brain tissues have been applied in neurosurgical simulations of human brain deformation (Warfield et al., 2000). To improve the accuracy of simulating cortical folding as a deformation process with higher strains, nonlinear constitutive properties of soft tissues are known to be more realistic than their linear counterparts (Malvern, 1969; Spencer, 1980; Fung, 1993; Bathe, 1996). Nonlinear simulations of brain deformation have been used in neurosurgery applications in order to improve pre-operative to intra-operative image registration (Hagemann and Rohr, 1999; Wittek et al., 2007), as well as for modelling the deformation of other soft tissues (Nash and Hunter, 2000; Pathmanathan et al., 2004; Fernandez and Hunter, 2005).

Further to these mathematical extensions for future modelling of cortical folding, biomechanical experiments on developing brain tissue must be conducted to explicitly measure the gray and white matter internal forces and elasticity properties. These studies have been conducted for adult brain tissue (Velardi et al., 2006) and a number of developing brain tissue (Thibault and Margulies, 1998; Miller and Chinzei, 2002; Prange and Margulies, 2002; Gefen et al., 2006). Such knowledge will allow the biomechanical properties to be assigned without need to borrow or extrapolate from mature brain tissue values, which will result in more realistic exploration of cortical folding mechanisms. Our finding that sulci form in regions of low FA, as observed in the MRI data, remains to be verified via histological analysis of white matter development. In this study we focused on modelling and simulation of an initial cortical geometry and particular loadings and constraints for the proposed models. The scarcity of data is due to the annual mating and long gestational term of sheep, as well as the unusually long MRI data acquisition time (50–60 h for each brain). In the future, we intend to extend the simulations to more extensive 3D cortical folding based on MRI data from additional cortical regions. In addition, MRI brain images from in utero and preterm human neonates are becoming available (Grossman et al., 2006; Dubois et al., 2008), which may be used for modelling brain development in the future.

6. Conclusion

This study of the biomechanisms involved in cortical folding has incorporated realistic cortical geometry of developing fetal sheep brains, an explicit cortical growth mechanism, cues to variable white matter fibre tension via external tensile forces, and realistic biomechanical properties of white and gray matter. Novel use of MRI data of a series of fetal sheep brains has led to the characterization of structural and diffusivity changes across key developmental time points. Our cortical growth model, formulated as a time-dependent, large deformation, solid stress–strain model of the fetal sheep brain at 70 days gestation, introduces the use of osmotic expansion as an analogy for tangential growth of the cortex. By simulating variability in white matter elasticity consistent with the measured experimental diffusion anisotropy variability in the white matter, we have demonstrated that tangential cortical growth is a plausible biomechanism of sulcal root formation and hence cortical folding.

References

Altenbach, H., Altenbach, J., Kissing, W., 2004. Mechanics of Composite Structural Elements. Springer-Verlag, New York.

Basser, P.J., Mattiello, J., LeBihan, D., 1994. MR diffusion tensor spectroscopy and imaging. Biophysical Journal 66, 259–267.

Bathe, K.J., 1996. Finite Element Procedures. Prentice Hall, New Jersey.

Boresi, A.P., Chong, K.P., 1987. Elasticity in Engineering Mechanics. Elsevier, New York.

Buettner-Janusch, J., 1963. Evolutionary and Genetic Biology of Primates, vol. 1. Academic Press, New York.

Cachia, A., Mangin, J.F., Riviere, D., Papadopoulos-Orfanos, D., Kherif, F., Bloch, I., Regis, J., 2003. A primal sketch of the cortex mean curvature: a morphogenesis based approach to study the variability of the folding patterns. IEEE Transactions on Medical Imaging 22, 754–765.

Camara, O., Schweiger, M., Scahill, R.I., Crum, W.R., Sneller, B.I., Schnabel, J.A., Ridgway, G.R., Cash, D.M., Hill, D.L.G., Fox, N.C., 2006. Phenomenological model of diffuse global and regional atrophy using finite element methods. IEEE Transactions on Medical Imaging 25 (11), 1417–1429.

Cartwright, J., 2002. Labyrinthine turing pattern formation in the cerebral cortex. Journal of Theoretical Biology 217, 97–103.

Dale, A.M., Fischl, B., Sereno, M.I., 1999. Cortical surface-based analysis: I. Segmentation and surface reconstruction. NeuroImage 9, 179–194.

Dubois, J., Benders, M., Cachia, A., Lazeyras, F., Leuchter, R.H.-V., Sizonenko, S.V., Borradori-Tolsa, C., Mangin, J.F., Hüppi, P.S., 2008. Mapping the early cortical folding process in the preterm newborn brain. Cerebral Cortex 18, 1444–1454.

Fernandez, J.W., Hunter, P.J., 2005. An anatomically based patient-specific finite element model of patella articulation: towards a diagnostic tool. Biomechanics and Modeling in Mechanobiology 4, 20–38.

Fischl, B., Sereno, M.I., Dale, A.M., 1999. Cortical surface-based analysis II: Inflation, flattening, and a surface-based coordinate system. NeuroImage 9, 195–207.

Fung, Y.C., 1993. Biomechanics: Mechanical Properties of Living Tissues, second ed. Springer-Verlag, New York.

Fung, Y.C., Tong, P., 2001. Classical and Computational Solid Mechanics. World Scientific, Singapore.

Gao, C., Tay, F.E.H., Nowinski, W.L., 2006. Modelling of the human brain with detailed anatomy for numerical simulation of surgical interventions. Journal of Physics: Conference Series 34, 985–989.

Garel, C., Chantrel, E., Brisse, H., Elmaleh, M., Luton, D., Oury, J.F., Sebag, G., Hassan, M., 2001. Fetal cerebral cortex: normal gestational landmarks identified using prenatal MR imaging. American Journal of Neuroradiology 22, 184–189.

Gefen, A., Gefen, N., Zhu, Q., Raghupathi, R., Margulies, S.S., 2006. Agedependent changes in material properties of the brain and braincase of the rat. Biomechanics and Modeling in Mechanobiology 5, 53–61.

Geng, G., Johnston, L., Yan, E., Walker, D., Egan, G., 2007. Modelling cerebral cortical folding. In: Proceedings of Workshop on Computational Biomechanisms, International Conference on Medical Image Computing and Computer Assisted Intervention. pp. 55–64.

Grossman, R., Hoffman, C., Mardor, Y., Biegon, A., 2006. Quantitative MRI measurements of human fetal brain development in utero. NeuroImage 33, 463–470.

Hagemann, A., Rohr, K., 1999. Biomechanical modelling of the human head for physically based, nonrigid image registration. IEEE Transaction on Medical Imaging 18 (10), 875–884.

Hilgetag, L.C., Barbas, H., 2005. Developmental mechanics of the primate cerebral cortex. Anatomy and Embryology 210, 411–417.

Kroenke, C.D., Essen, D.C.V., Inder, T.E., Rees, S., Bretthorst, G.L., Neil, J.J., 2007. Microstructural changes of the baboon cerebral cortex during gestational development reflected in magnetic resonance imaging diffusion anisotropy. Journal of Neuroscience 27, 12506–12515.

Levine, D., Barnes, P.D., 1999. Cortical maturation in normal and abnormal fetuses as assessed with prenatal MR imaging. Radiology 210, 751–758.

Malvern, L.E., 1969. Introduction to the Mechanics of a Continuous Medium. Prentice Hall (p. 273).

Mangin, J.F., Riviere, D., Cachia, A., Duchesnay, E., Cointepas, Y., Papadopoulos-Orfanos, D., Scifo, P., Ochiai, T., Brunelle, F., Regise, J., 2004. A framework of study the cortical folding patterns. NeuroImage 23, S129–S138.

Meyer, G., 2007. Genetic Control of Neuronal Migrations in Human Cortical Development. Springer, Berlin.

Miller, K., Chinzei, K., 2002. Mechanical properties of brain tissue in tension. Journal of Biomechanics 35, 483–490.

Nash, M.P., Hunter, P.J., 2000. Computational mechanics of the heart. Journal of Elasticity 61, 113–141.

Neil, J., Shiran, S., McKinstry, R., Schefft, G., Snyder, A., Almli, C., 1998. Normal brain in human newborns: apparent diffusion coefficient and diffusion anisotropy measured by using diffusion tensor MR imaging. Radiology 209, 57–66.

Neville, L., Egan, R.A., 2005. Frequency and amplitude of elevation of cerebrospinal fluid resting pressure by the Valsalva maneuver. Canadian Journal of Ophthalmology 40, 775–777.

Ottoson, D., 1983. Physiology of the Nervous System. The Macmillan Press, London and Basingstoke.

Pathmanathan, P., Gavaghan, D., Whiteley, J., Brady, S.M., Nash, M., Nielsen, P., Rajagopal, V., 2004. Predicting tumour location by simulating large deformations of the breast using a 3D finite element model and nonlinear elasticity. In: International Conference on Medical Image Computing and Computer Assisted Intervention. pp. 217–224.

Pierpaoli, C., Basser, P.J., 1996. Toward a quantitative assessment of diffusion anisotropy. Magnetic Resonance in Medicine 36, 893–906.

Prange, M.T., Margulies, S.S., 2002. Regional, directional and age-dependent properties of the brain undergoing large deformation. Journal of Biomechanical Engineering 124, 244–252.

Raghavan, R., Lawton, W., Ranjan, S., Viswannathan, R., 1997. A continuum mechanics-based model for cortical growth. Journal of Theoretical Biology 187, 285–296.

Rakic, P., 1995. A small step for the cell, a giant leap for mankind: a hypothesis of neocortical expansion during evolution. Trends in Neuroscience 18, 383–388.

Richman, D.P., Stewart, R.M., Hutchinson, J.W., Caviness, J.V.S., 1975. Developmental model of brain convolutional development. Science 189 (4196), 18–21.

Spencer, A.J.M., 1980. Continuum Mechanics. Longman, New York.

Taylor, Z., Miller, K., 2004. Reassessment of brain elasticity for analysis of biomechanisms of hydrocephalus. Journal of Biomechanics 37, 1263–1269.

Thibault, K.L., Margulies, S.S., 1998. Age-dependent material properties of the porcine cerebrum: effect on pediatric inertial head injury criteria. Journal of Biomechanics 31, 1119–1126.

Todd, P.H., 1982. A geometric model for the cortical folding pattern of simple folded brains. Journal of Theoretical Biology 97, 529–538.

Toro, R., Burnod, Y., 2005. A morphogenetic model for the development of cortical convolutions. Cerebral Cortex 15, 1900–1913.

Vaccarino, F.M., Fagel, D.M., Ganat, Y., Maragnoli, M.E., Ment, L.R., Ohkubo, Y., Schwartz, M.L., Silbereis, J., Smith, K.M., 2007. Astroglial cells in development, regeneration, and repair. The Neuroscientist 13, 173–185.

Van Essen, D.C., 1997. A tension-based theory of morphogenesis and compact wiring in the central nervous system. Nature 385, 313–318.

Velardi, F., Fraternali, F., Angelillo, M., 2006. Anisotropic constitutive equations and experimental tensile behavior of brain tissue. Biomechanics and Modeling in Mechanobiology 5, 53–61.

Venita, J., 1996. Pathology in an infant with Down's syndrome and Tuberous Sclerosis. Pediatrics Neurology 15, 57–59.

Warfield, S.K., Ferrant, M., Gallez, X., Nabavi, A., Jolesz, F.A., Kikinis, R., 2000. Real-time biomechanical simulation of volumetric brain deformation for image guided neurosurgery. In: SC 2000: High Performance Networking and Computing Conference, vol. 230. pp. 1–16.

Wittek, A., Miller, K., Kikinis, R., Warfield, S.K., 2007. Patient-specific model of brain deformation: application to medical image registration. Journal of Biomechanics 40, 919–929.

Zhang, J., Richards, L.J., Yarowsky, P., Huang, H., van Zijl, P.C.M., Mori, S., 2003. Three-dimensional anatomical characterization of the developing mouse brain by diffusion tensor microimaging. NeuroImage 20, 1639–1648.